Analysis of the in-beam test of the EXL demonstrator @ GSI

A. Najafi, C. Rigollet, N. Kalantar, H. Moeini, J. Van de Walle

06 April 2010

Contents

Abstract

The EXL demonstrator test is done at FRagment Separator (FRS) at GSI. The vacuum chamber in this test measurement contains one DSSD and two Si(Li)s. In addition, there are two CsI scintillators, next to each other, at the back of the chamber, outside the vacuum. A beam of 100 MeV protons was used, and the energy was increased in the last hour of the experiment to 150 MeV. This report presents the results of a preliminary analysis of the data of 100 MeV beam energy, aiming at a better understanding of the detection system.

1 Introduction

EXotic nuclei studied in Light ion reactions (EXL), is an experiment focusing on the properties of unstable exotic nuclei. The aim of EXL is to study the structure of unstable exotic nuclei in light-ion scattering experiments at intermediate energies. The objective is to capitalise on light-ion reactions in inverse kinematics by using novel storage-ring techniques and a universal detector system providing high resolution and large solid angle coverage in kinematically complete measurements. The apparatus foreseen will be installed at the internal target position at the New Experimental Storage Ring (NESR). It comprises a silicon target-recoil detector for charged particles, complemented by γ ray and slow-neutron detectors, located around the internal gas-jet target, a forward detector for fast ejectiles (both charged particles and neutrons) and an in-ring heavy-ion spectrometer [1]. The overall design for the recoil and γ ray detector for EXL is divided in two major arrays, the Silicon Particle Array (ESPA) to detect light charged particles from the target and the Gamma and Particle Array (EGPA) to detect punch-through particles and γ rays.

A first test at KVI allowed to investigate the response and properties of one ESPA module. In a second phase we added two CsI crystals to make a complete module of the EXL target recoil detectors.

2 Experimental Setup

2.1 FRagment Separator

The projectile fragment separator, FRS, designed for research and applied studies with relativistic heavy ions was installed at GSI as a part of the high-energy SIS/ESR accelerator facility. The FRS is an achromatic magnetic forward spectrometer with a momentum resolving power of $p/\Delta p = 1500$ for an emittance of 20π mm mrad. Heavy ion beams with magnetic rigidities from 5 to 18 Tm can be analyzed by the device [2]. For the EXL demonstrator test measurement only half of the length of the FRS was used. The setup was mounted in the middle of the FRS. For the present measurement, a beam of 100 MeV protons was injected from SIS 18 into the FRS. In the last 40 minutes of the beam time, the energy of the beam was increased to 150 MeV. Fig. 1 shows the beam-line setup of the FRS and the red spot on the beam-line indicates the location of EXL demonstrator setup.

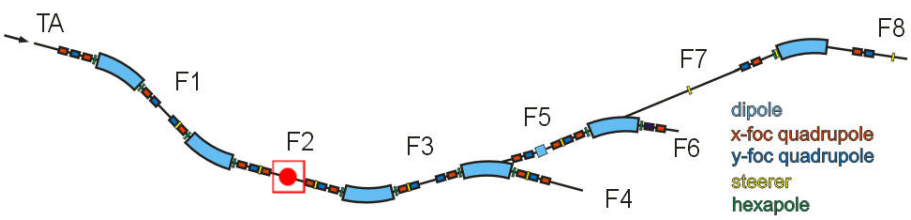

Figure 1: The FRS beam-line setup at GSI, Darmstadt, Germany. The red spot shows the location of EXL demonstrator setup.

2.2 Detection system

The detection system is rather simple. The beam emerging from the FRS beam pipe passes through ∼10 cm of air and enters the vacuum chamber through a thin Mylar foil. Vacuum inside the chamber is in the order of 10^{-5} mbar. This chamber contains a Double-sided Strip Silicon Detector (DSSD) followed by two Lithium-drifted Silicon detectors (Si(Li)s), which are cooled to a subzero temperature. The beam punches through all of these detectors and exits the chamber through a thin steel foil, to stop in two CsI scintillators placed at the back of the chamber. These scintillators represent

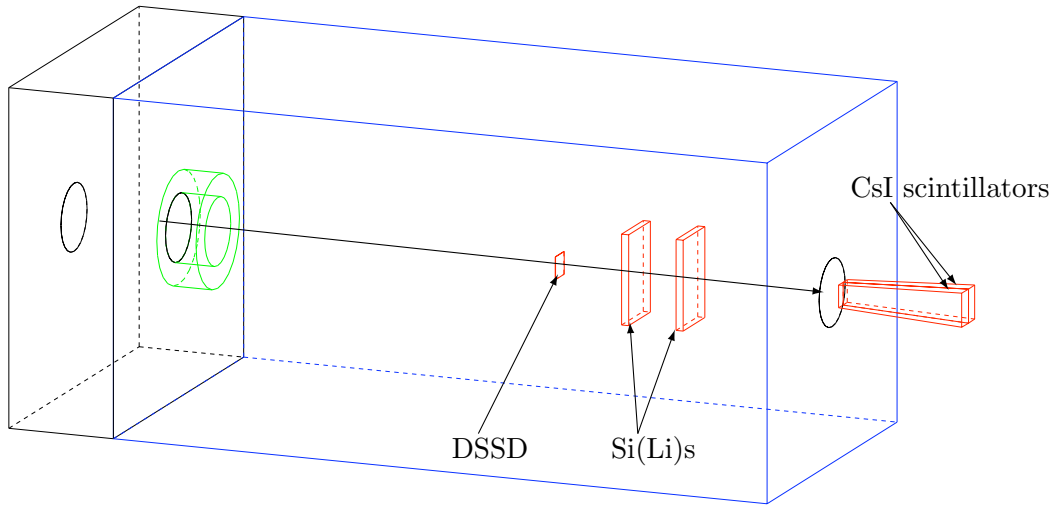

Figure 2: The geometry of the detectors in EXL demonstrator test.

a module of EGPA. Fig. 2 shows a schematic view of the setup. The red volumes are detectors and the line in the middle is the beam line. The details of the detectors and their geometry is described in the following sections.

Double-sided Silicon Strip Detector (DSSD)

The main purpose of using a DSSD is the tracking of the particle trajectories. From the name, it is clear that a DSSD is composed of an array of strips on each side of a thin silicon detector. The DSSD used in this experiment has 64 strips on the front side and 64 strips on the rear side. During the experiment, each four strips were connected to a single output channel, thus transforming the 64×64 strips detector into 16×16. The dimensions of the active area of the DSSD are $21 \times 21 \times 0.3$ mm^3.

Lithium-drifted Silicon detector (Si(Li))

The lithium-drifted silicon detectors are used to measure the energy of particles and act as a ΔE detector of a $\Delta E - E$ system. In this experiment, two Si(Li)s were mounted inside the chamber. The dimensions of the Si(Li) are $80 \times 50 \times 6.5$ mm^3. The first Si(Li) was installed 8 cm downstream of the DSSD, and was centered in the beam path. The second one was placed off-center, in a way that the beam shines only on one pad. A schematic picture of Si(Li)s is illustrated in Fig. 3 (left), and the right picture shows a photograph of one of the Si(Li)s used in the experiment.

CsI scintillator

Two CsI crystals are used for the calorimeter part of the system. Each crystal is wrapped in a foil and they are placed next to each other outside the vacuum chamber at a distance of 26 cm downstream of the DSSD. The beam stops in the scintillators. Fig. 4 shows a photo of two scintillator crystals placed in the holder to be mounted at the back of the vacuum chamber.

3 Data analysis

The main goal of the test experiment was to understand the detection system and the data acquisition system. Therefore, after calibration, it is necessary to have a reasonable

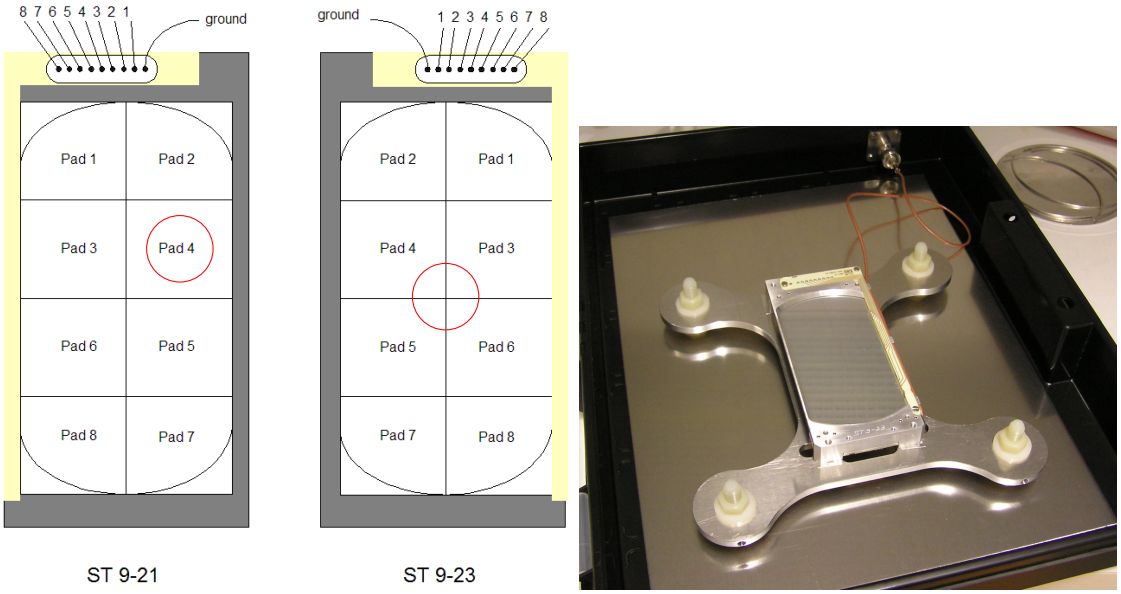

Figure 3: The Lithium-drifted silicon detectors (Si(Li)) used in the experiment. Left: A schematic picture of the Si(Li)s; The circles show the approximate location of the beam spot. Right: A photograph of a Si(Li), used in experiment.

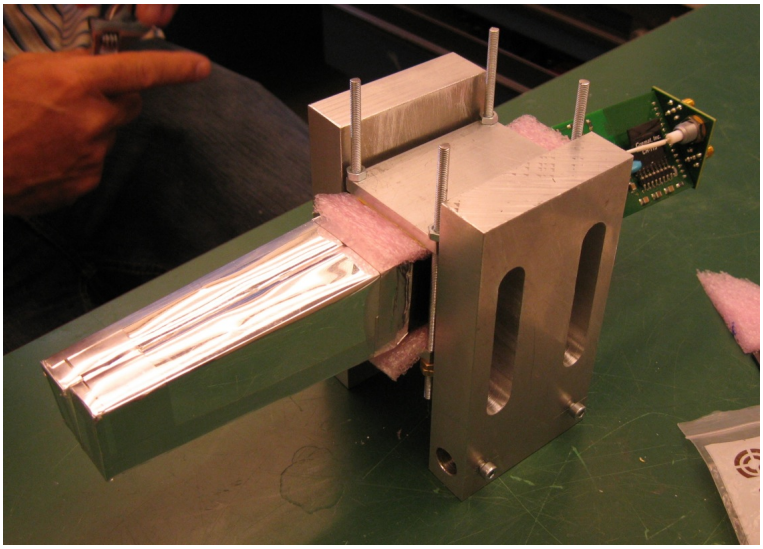

Figure 4: The CsI scintillator crystals placed in the holder.

description of the behaviour of the spectra of different detectors. The calibration process relies on the use of radioactive sources, emitting γ rays and α particles with known energies, but also on cosmic ray for larger energy ranges. When examining the data, it became clear that radioactive sources and cosmic ray data do not provide enough calibration points. Therefore, we decided to use simulations results as a third tool for calibration. In the next section the simulation of the experiment is introduced briefly and in the following sections the calibration of different detectors is discussed and then the behaviour of the spectra is described.

3.1 Simulation

A simplified version of the experiment is simulated using Geant4. The defined geometry in simulation is roughly the same as the real experiment, except that the Si(Li)s are defined as made of Silicon only. Also the DSSD is defined as a thin silicon detector without any strips. The simulated geometry is shown in Fig. 2 and table 1 shows the energy deposit of a beam of 100 MeV protons in each detector. The centroid energy and the FWHM are obtained from a Gaussian fit of the spectrum of each detector.

With this geometry, another simulation is performed. In order to have a good evalu-

Detector	Energy deposit [MeV]	FWHM
DSSD	0.37	0.13
Si(Li)#1	8.70	0.87
Si(Li)#2	9.79	0.88
CsI#1 & #2	80.8	1.35

Table 1: The energy deposit of a beam of 100 MeV protons in each detector of the setup.

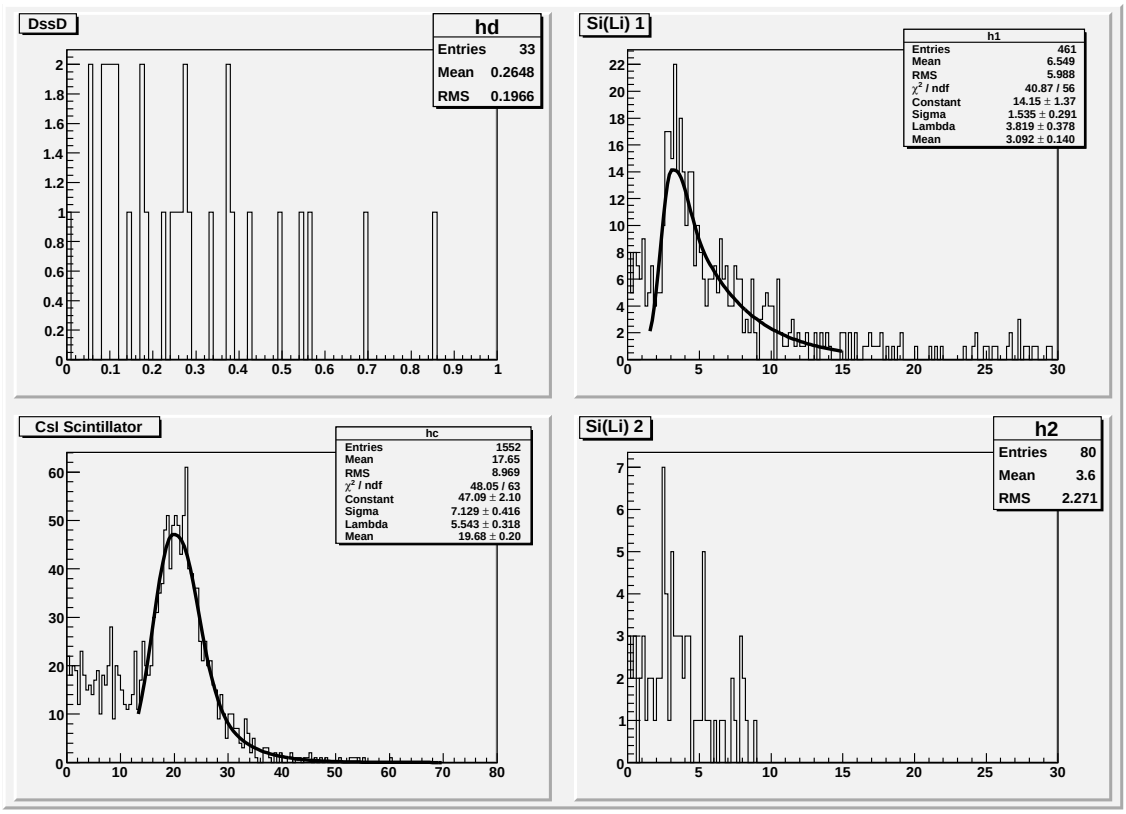

Figure 5: Simulation of cosmic muons on different detectors of the setup.

ation of the energy deposited by cosmic muons in the detectors, a particle gun is defined to generate muons. The distribution of the location of the gun, is randomly generated with $\cos^2(\theta)$ weight, on a hemisphere of 5 m radius. The energy of muons is generated randomly within the interval 0.4 to 1.4 GeV. The results of a run of 50 million events is depicted in Fig. 5. Since in the experiment only one pad of the second Si(Li) was read out by the data acqusition system, the dimensions of the second Si(Li) in the simulation, was changed to the dimensions of one pad, which is $22 \times 22 \times 6.5$ mm^3. Because of the smaller size, there was less number of events on this Si(Li) (see Fig. 5). Refinement of this simulation is being done, in order to create better statistics.

3.2 Calibration of DSSD

The DSSD has 16 output channels on the front and the rear sides. Therefore, the calibration is needed for 32 output channels of the DSSD. There was an ^{241}Am source placed in front of the DSSD in the vacuum chamber. The dominant decay mode of this source is the emission of an α particle with an energy of 5.49 MeV [3]. The calibration of the DSSD is done using the peak due to the α particles and also the simulation with beam. Fig. 6 shows the spectra of the first 16 channels of the DSSD, using this calibration. In each plot, there are two peaks. The peak at lower energies is due to the beam, and the one at higher energies is due to the radioactive source.

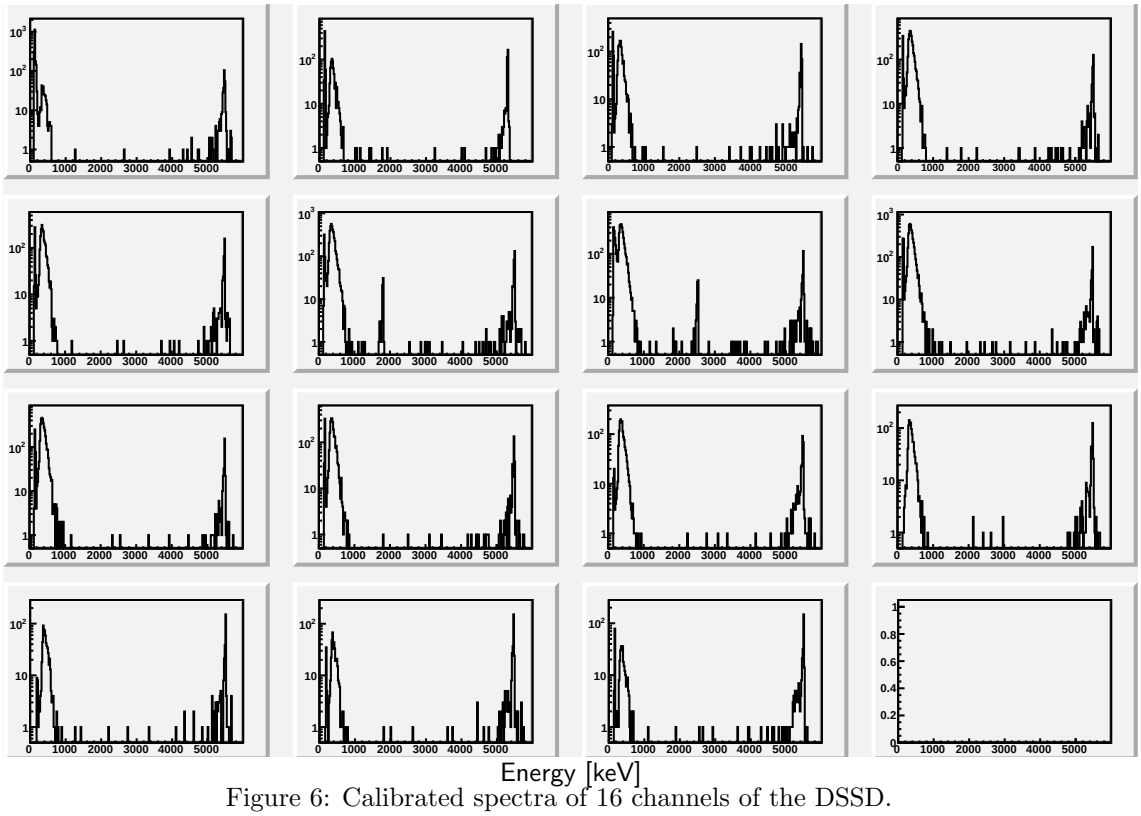

Figure 6: Calibrated spectra of 16 channels of the DSSD.

3.3 Calibration of Si(Li)

Fig. 7 shows the raw spectrum of Si(Li)#2 in the calibration run, i.e. taking data without beam. There is a clear peak at the channel number around 800, which is due to the radioactive source, placed in front of the Si(Li). The source is ^{148}Gd and its only decay mode is the emission of an α particle with an energy of 3.182 MeV [4]. In order to have an absolute calibration we need one more calibration point. Therefore, we sought for another peak due to the cosmic muons. At this step we used the results of the simulation of cosmic muons in the geometry of the experimental setup (see Fig. 5). Simulations show that the energy deposit of cosmic muons in Si(Li) has a peak of 3 MeV, which falls on top of the peak from the source. Therefore, we can't use cosmic rays as a source of calibration. In addition to the peak at the channel number around 800, a small peak around 1600 can be recognized. At the moment, the origin of this peak is still unknown.

Finally, we used the radioactive source peak and the simulation with beam as two necessary calibration points. Therefore, we can not provide an absolute value for the reconstruction of the total energy. Fig. 8 shows the calibrated spectrum of the Si(Li)#2.

Unfortunately, the first Si(Li) was not operational because of a broken connection. Therefore, we don't have any data to analyze from that Si(Li).

3.4 CsI scintillators data

During the experiment, there was a ^{60}Co source placed in front of the CsI scintillators. However, the energy of the emitted γ rays is 1.3 MeV [5], which is very low compared to the range of energies we expect in the scintillators, which are few tens of MeV (see table 1). Therefore, we don't have enough information for the calibration of the scintillators.

In Fig. 9 the spectrum of one of the CsI crystals is plotted. There are two clear peaks in the spectrum. The second peak, at higher energy is due to the beam. However, the origin of the peak at lower energy was unknown until I did some tests. I applied very restrictive conditions on the observed events in the CsI spectrum, to choose only signals due to the FRS beam. Nevertheless, two peaks still remain, with almost the same height. The applied conditions include:

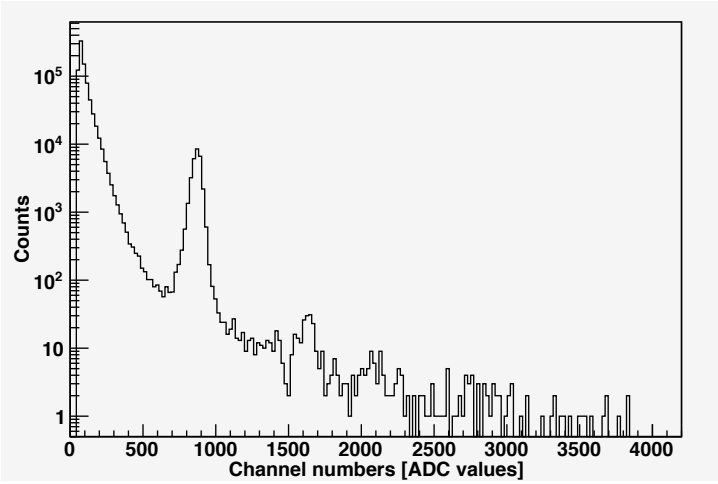

Figure 7: The raw spectrum of Si(Li)#2 resulting from calibration run, i.e. no beam from FRS.

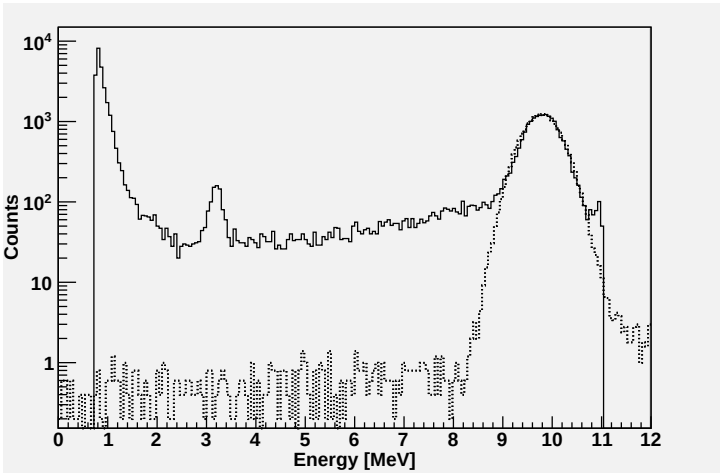

Figure 8: The spectrum of Si(Li)#2; The solid curve shows the experimental data calibrated using radioactive source and simulation. The dotted curve shows the result of the simulation of the demonstrator with a beam of 100 MeV protons.

- hit on Si(Li) with an energy deposit in the range of the energy deposit by the beam (see table 1),
- hit on a small region selected in DSSD. Three regions with low, high and medium count rates are selected, which represent the edge of the beam, the center and somewhere in between, respectively.

Fig. 10 shows the results of these conditions for CsI#1. The first, second and third rows show the results of low, medium and high count rate conditions, respectively. The two peak structures are clear in all situations. It implies that the peak at lower energy originates from the beam as well as the other one. One possible explanation could be a light leakage between the crystals.

Despite the fact that each crystal is wrapped in an opaque foil, a considerable amount of scintillation light leaks to the neighboring crystal. The leaked light produces the first peak in Fig. 9, which has about the same height as the second peak.

More investigations show that this explanation of the low energy peak of the CsI scintillators doesn't account for 100% of the peak intensity. Fig. 11 shows CsI#1 data with the conditions that both DSSD and Si(Li) are hit and that the CsI#2 does not detect anything. These conditions should kill the light leakage completely, but they don't. Therefore, one or more phenomena contribute to this low energy peak.

To quantify this contribution, I constrained the data, such as the ones shown in Fig. 9 for a particular CsI scintillator, to the low energy peak and I read the number of

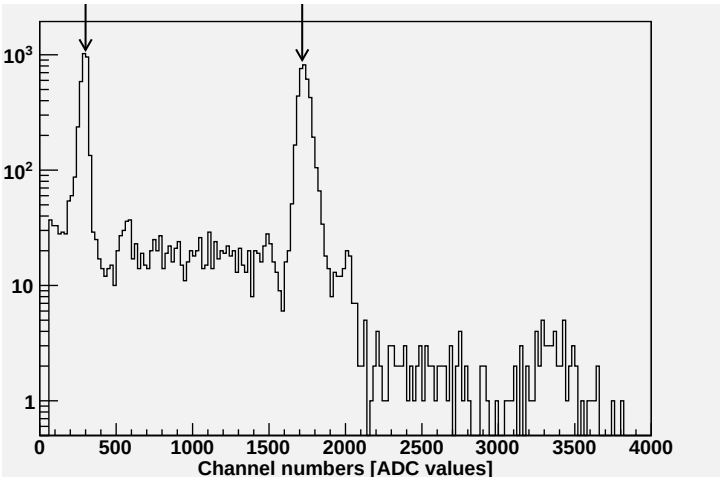

Figure 9: The raw spectrum of the CsI#1 scintillator; two peaks are distinctly observed.

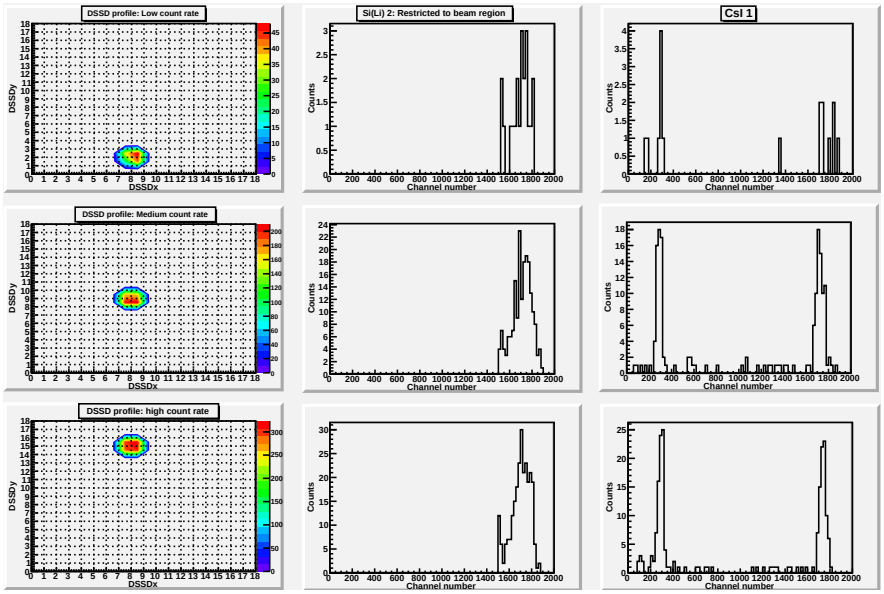

Figure 10: The results of applying restrictive conditions to the data of CsI#1. The left column shows the section of the beam chosen by the DSSD. The column in the middle shows the region of energy as measured by the Si(Li). And the right column shows the result of these conditions on CsI#1 spectrum.

remaining events in two different situations: first, without any condition on the other CsI (Fig. 12, left) and second with the condition that the other CsI does not detect anything (Fig. 12, right). Comparison of these two numbers gives rise to a 1.7% contribution from a yet unknown effect.

Fig. 13 illustrates a more clear pattern of the above points about the light leakage between the CsI crystals. Obviously the projection of the picture on each one of the side axes gives two peaks in the spectra of the CsI scintillators. The events in the two marked peaks are the events, that have created the light leakage, because they have a non-zero energy deposit in both of the scintillators. This indicates that always a fraction of the scintillated light is penetrating to the neighboring crystal through the wrapping foils, and therefore, for each hit in one of the crystals there is a small signal in the neighboring crystal. Additionally, the dotted arrow in the Fig. 13 illustrates that the leakage is increasing linearly with the energy of the incoming particles, which agrees with our description of this phenomenon.

Although some aspects of the data of the CsI scintillators are revealed using Fig. 13, this figure still has a confusing point. There is a considerable number of events right on the axis of CsI#2, and also on the CsI#1 axis. These events are detected by only one

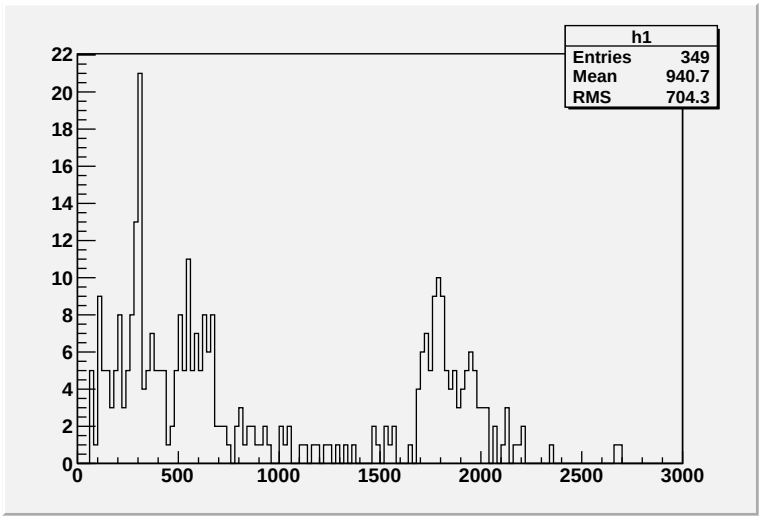

Figure 11: CsI#1 data restricted to three conditions: CsI#2 has not detected anything AND the signal has a hit on the Si(Li) AND one of the strips of DSSD.

of the crystals. If these on-axis events create a light leakage, the peak of these events should be almost at the same channel number as the corresponding peaks, marked by the arrows. But if they do not create any light leakage, we expect the peak of the on-axis events to be at a larger channel number than the peak of the events, creating light leakage. To clarify this point, a test was done, as following.

Peak#1 in Fig. 13 was chosen and then it was projected on the axis of the CsI#2. The result of this operation is depicted in Fig. 14, left panel, and the resulting projection is depicted as a gray solid curve in Fig. 15. Additionally, the on-axis events are put in a one dimensional histogram. The right panel in Fig. 14 shows these events and the resulting histogram is depicted as a dashed black curve in Fig. 15. It is clear that the peak of the dashed curve is not at larger channels (if anything it is located at a smaller channel number). Therefore, we conclude that the on-axis events are sharing the light leakage effect, but because of a yet unknown effect the leaked light is not detected.

4 Conclusions

Since we had only one DSSD in this test experiment we can't track the beam particles. In future experiments, we should add another DSSD, for this purpose. For the total energy reconstruction we should know the amount of energy loss of the beam in the DSSD. Therefore, the energy calibration of the DSSD strips was done. The average energy resolution of the strips is 30% at an average energy of 370 keV.

With a Gaussian fit of the Si(Li) spectrum in Fig. 8, we see that the energy resolution

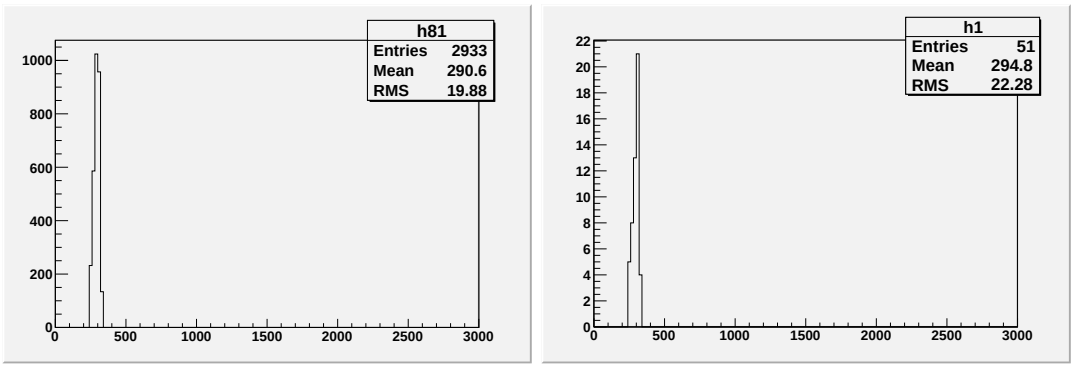

Figure 12: CsI#1 data restricted to beam selection conditions; Left: without any condition on CsI#2, Right: with condition that CsI#2 does not detect anything.

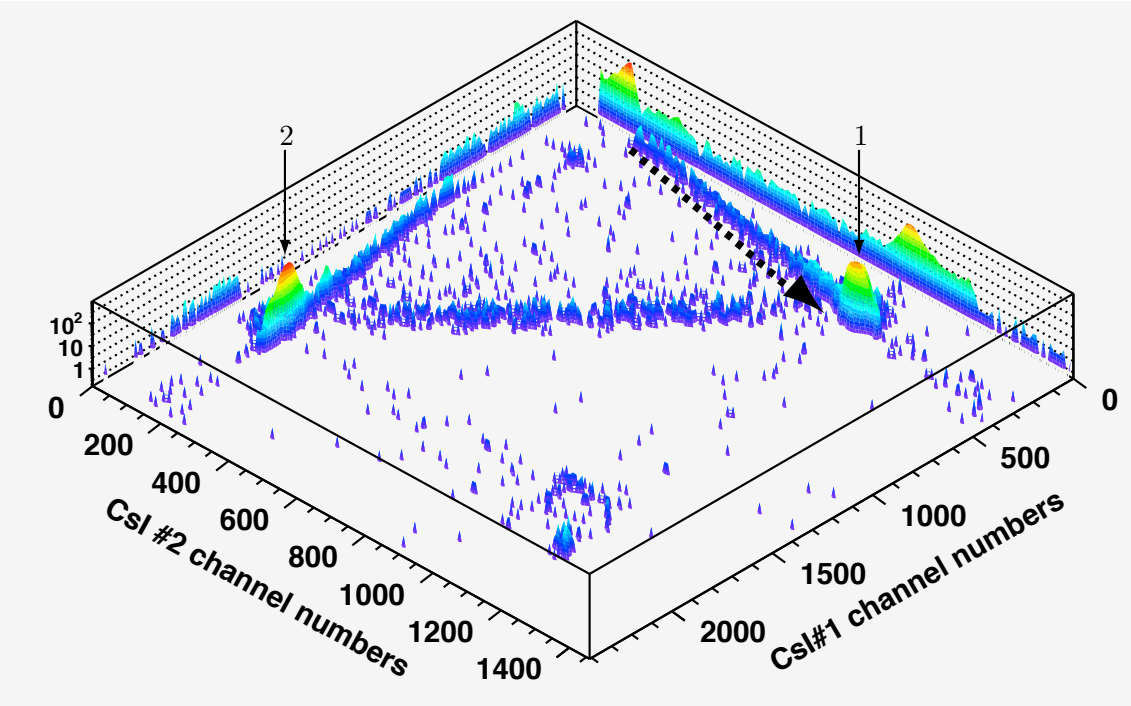

Figure 13: The three dimensional view of CsI#2 channel numbers versus CsI#1 channel numbers. The two peaks, indicated by the vertical arrows show the light leakage between two scintillators. The thick dotted arrow, shows the linear increase of the light leakage with the increase of the energy of the incoming particle.

of the Si(Li) is 8.5% at $E = 9.79$ MeV. Since the exact amount of energy deposited in the Si(Li) is of great importance we should calibrate the Si(Li)s accurately, and independent of simulations. Therefore, in the future experiments we should use a radioactive source of particles, with energy deposit of which, in the Si(Li) is different from the energy deposit of the cosmic muons. In this way, we are able to use the cosmic ray data as a second calibration point. Or as a second way, adding another radioactive source, that emits particles with different energy would result in another calibration point and eventually a much better calibration. This is due to the fact that, the cosmic ray spectra usually have a broad peak in comparison to the spectra of the radioactive sources.

It is clear that we need more efficient information about the behavior of the calorimeter of the experiment. Especially, we should investigate the effect of light leakage between the CsI scintillators.

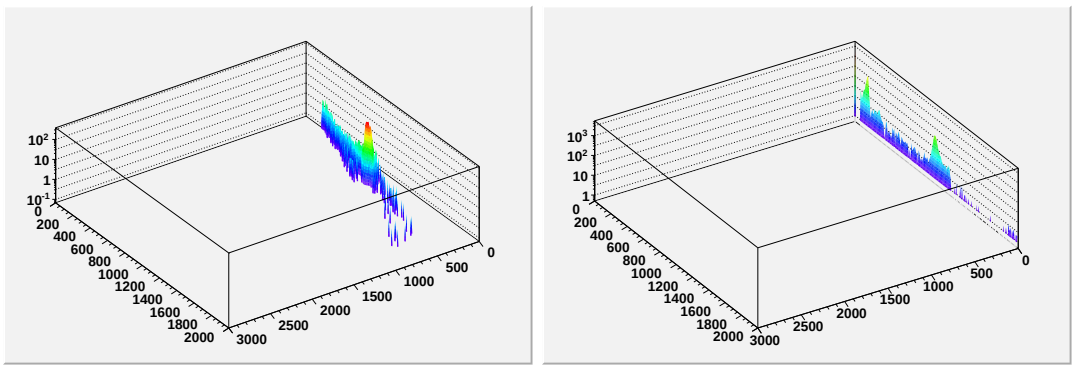

Figure 14: CsI#2 channel numbers versus CsI#1 channel numbers; left, subjected to a constraint, that cuts all the events but the ones forming the depicted peak and the linear tail; right, subjected to the on-axis events of the CsI#2 scintillator.

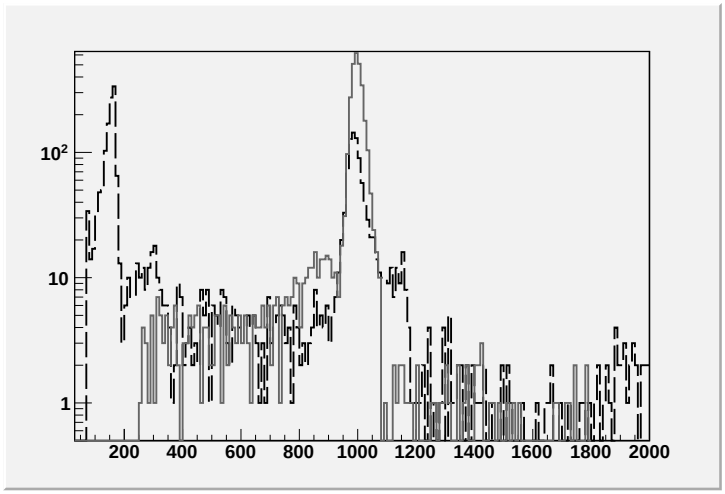

Figure 15: The projections of the left (right) histograms in Fig. 14 on the CsI#2 axis results in the solid gray (dashed black) curve.

Bibliography

[1] Technical proposal of the EXL project.
http://www-linux.gsi.de/~wwwnusta/tech_report/05-exl.pdf

[2] H. Geissel *et al.*, Nucl. Instr. and Meth. Phys. Res. **B70** (1992) 286-297.

[3] M. S. Basunia, Nuclear Data Sheets 107, 3323 (2006).

[4] M. R. Bhat, Nuclear Data Sheets 89, 797 (2000).

[5] J. K. Tuli, Nuclear Data Sheets 100, 347 (2003).